https://doi.org/10.5194/acp-2022-376
Preprint. Discussion started: 8 June 2022

Atmospheric Chemistry and Physics Discussions

Oligomer formation from the gas-phase reactions of Criegee intermediates with hydroperoxide esters: mechanism and kinetics

Long Chen,[1,2] Yu Huang,*[1,2] Yonggang Xue,[1,2] Zhihui Jia,[3] Wenliang Wang[4]

[1] *State Key Lab of Loess and Quaternary Geology (SKLLQG), Institute of Earth Environment, Chinese Academy of Sciences (CAS), Xi'an, 710061, China*

[2] *CAS Center for Excellence in Quaternary Science and Global Change, Xi'an, 710061, China*

[3] *School of Materials Science and Engineering, Shaanxi Normal University, Xi'an, Shaanxi, 710119, China*

[4] *School of Chemistry and Chemical Engineering, Key Laboratory for Macromolecular Science of Shaanxi Province, Shaanxi Normal University, Xi'an, Shaanxi, 710119, China*

Submitted to *Atmospheric Chemistry & Physics*

*Corresponding author:
Prof. Yu Huang, E-mail address: huangyu@ieecas.cn

https://doi.org/10.5194/acp-2022-376
Preprint. Discussion started: 8 June 2022

Atmospheric Chemistry and Physics Discussions

Abstract

Hydroperoxide esters, formed in the reactions of carbonyl oxides (also called Criegee intermediates, CIs) with formic acid, play a crucial role in the formation of secondary organic aerosol (SOA) in the atmosphere. However, the transformation mechanism of hydroperoxide esters in the presence of stabilized Criegee intermediates (SCIs) is not well understood. Herein, the oligomerization reaction mechanisms and kinetics of distinct SCIs (CH_2OO, *syn*-CH_3CHOO, *anti*-CH_3CHOO and $(CH_3)_2COO$) reactions with their respective hydroperoxide esters as well as with hydroperoxymethyl formate (HPMF) are investigated in the gas phase using quantum chemical and kinetics modeling methods. The calculations show that the addition reactions of SCIs with hydroperoxide esters proceed through successive insertion of SCIs into hydroperoxide ester to form oligomers that involve SCIs as the repeating unit. The exothermicity of oligomerization reactions significantly decreases when the number of methyl substituents increases, and the exothermicity of *anti*-methyl substituted carbonyl oxides is obviously higher than that of *syn*-methyl substituted carbonyl oxides. The –OOH insertion reaction is energetically more feasible than the –CH insertion pathway in the SCIs oligomerization reactions, and the barrier heights increase with increasing the number of SCIs except *syn*-CH_3CHOO. For the reactions of distinct SCIs with HPMF, the barrier of –OOH insertion pathway shows a dramatic decrease when a methyl substituent occurs at the *anti*-position, while it reveals a significant increase when a methyl group is introduced at the *syn*-position and dimethyl substitutions. Compared with the rate coefficients of the CH_2OO + HPMF reaction, the rate coefficients increase by about one order of magnitude when a methyl substituent occurs at the *anti*-position, whereas the rate coefficients decrease by 1-2 orders of magnitude when a methyl group is introduced at the *syn*-position. These new findings advance our current understanding on the influence of Criegee-chemistry on the formation processes and chemical compositions of SOA.

https://doi.org/10.5194/acp-2022-376
Preprint. Discussion started: 8 June 2022

Atmospheric Chemistry and Physics Discussions

1. Introduction

Alkenes are an important class of volatile organic compounds (VOCs) that are emitted into the atmosphere from large quantities of biogenic and anthropogenic sources (Lester and Klippenstein, 2018). The reaction with ozone is one of the dominant degradation pathways for alkenes in the atmosphere (Johnson and Marston, 2008; Atkinson and Arey, 2003). Ozonolysis of alkene proceeds through the electrophilic 1,3-cycloaddition of ozone to C=C double bond of alkenes to form a primary ozonides (POZ), and then it rapidly decomposes into a carbonyl compound and a carbonyl oxide (also called Criegee intermediates, CIs) (Criegee, 1975; Osborn and Taatjes, 2015; Giorio et al., 2017). A part of the initially energized CIs (~ 37-50%) may promptly dissociate to OH radicals, which are thought to be an important nonphotolytic source of OH radicals in the atmosphere (Novelli et al., 2014; Liu et al., 2014). The remaining CIs (~ 63-50%) are collisionally stabilized prior to the thermal unimolecular decay (Lester and Klippenstein, 2018; Novelli et al., 2014; Anglada and Solé, 2016). The stabilized Criegee intermediates (SCIs) can proceed bimolecular reactions with various trace species such as H_2O, NO_2, SO_2, and HCOOH to generate secondary organic aerosol (SOA), thus profoundly influencing air quality, global climate and human health (Osborn and Taatjes, 2015; Khan et al., 2018; Lin and Chao, 2017; Liu et al., 2019; Chhantyal-Pun et al., 2018; Gong and Chen, 2021; Taatjes, 2017).

Formic acid (HCOOH), one of the most abundant carboxylic acids, has a significant influence on rainwater acidity in remote areas, where pH reduces by 0.25-0.5 in the presence of HCOOH (Stavrakou et al., 2012; Wang et al., 2020; Chaliyakunnel et al., 2016). It also plays an important role in the formation of cloud condensation nuclei (CCN), indirectly influencing radiative forcing and climate change (Yu, 2000). The primary sources of HCOOH include biomass burning, human activities, tropical and boreal forests, as well as the secondary sources involve the photochemical oxidation of non-methane hydrocarbons, such as ketene-enols, vinyl alcohol, isoprene, and terpenoids (Stavrakou et al., 2012; Wang et al., 2020;

https://doi.org/10.5194/acp-2022-376
Preprint. Discussion started: 8 June 2022


Atmospheric Chemistry and Physics Discussions

Chaliyakunnel et al., 2016; So et al., 2014; Paulot et al., 2011). According to satellite measurements, the production of HCOOH is up to 100-120 Tg yr^{-1}, and the value is expected to increase due to the acceleration of industrialization and urbanization (Stavrakou et al., 2012). Recent kinetics measurements have revealed that the reaction with HCOOH is a more important loss process for SCI than is presently assumed, especially in terrestrial equatorial areas and in high SCI concentration areas (Welz et al., 2014; Chung et al., 2019). The formed hydroperoxide esters have been identified as the low-volatility and high-oxygenated compounds, contributing to the formation and growth of SOA (Welz et al., 2014; Vansco et al., 2021; Sakamoto et al., 2017; Riva et al., 2017).

Welz et al. (2014) directly determined the rate coefficients for the reactions of CH_2OO and CH_3CHOO with formic and acetic acid by employing multiplexed photoionization mass spectrometry and cavity-enhanced broadband ultraviolet absorption spectroscopy. They found that the measured rate coefficients are in the excess of 1.0×10^{-10} cm^3 $molecule^{-1}$ s^{-1}, which are several orders of magnitude greater than those derived from previous experimental studies (Johnson et al., 2001; Tobias et al., 2001). Sipilä et al. conducted a competitive reaction kinetics experiment to investigate the reactions of acetone oxide ($(CH_3)_2OO$) with SO_2, HCOOH and CH_3COOH, and they concluded that the $(CH_3)_2OO$ + HCOOH/CH_3OOH reactions are faster than the $(CH_3)_2OO$ + SO_2 system by about three times (Sipilä et al., 2014). These high rate coefficients could make the reaction with carboxylic acids a substantial dominant chemical sink for carbonyl oxides in the atmosphere (Welz et al., 2014; Taatjes et al., 2019; Chhantyal-Pun et al., 2017). Quantum chemical calculations show that the reaction of CH_2OO with HCOOH proceeds through a facile transfer of hydrogen atom from the acidic OH group to the terminal oxygen of CH_2OO to form hydroperoxymethyl formate (HPMF) (Long et al., 2009; Vereecken, 2017; Porterfield et al., 2019). Chen et al. (2018) concluded the same by investigating the reactions of various carbonyl oxides with HCOOH that the barrierless 1,4-insertion reaction is the most favorable pathway, and the primary products are hydroperoxide esters. Caravan et al. (2020) employed high-level ab initio

https://doi.org/10.5194/acp-2022-376
Preprint. Discussion started: 8 June 2022


Atmospheric Chemistry and Physics Discussions

CCSD(T)-F12 methods to study the reaction of methyl vinyl ketone oxide (MVK-oxide) with HCOOH, and they found that the barrierless net insertion of MVK-oxide into HCOOH leading to the formation of a functionalized hydroperoxide is dominant over fragmentation to produce an alkoxy radical and OH radicals. Moreover, oligomerization reactions with hydroperoxides and peroxy radicals are identified as one of the dominant loss processes for carbonyl oxides under atmospheric conditions (Sakamoto et al., 2013; Sadezky et al., 2008; Zhao et al., 2015; Chen et al., 2017 and 2019; Rousso et al., 2018). All the above milestone investigations provide important information for understanding the chemistry of Criegee intermediate in the presence of carboxylic acids. However, to the best of our knowledge, there are few studies on the oligomerization reactions of SCIs with hydroperoxide esters, which are important with regard to organic new particle and cloud condensation nuclei formations. Moreover, the relationship between the reactivity of SCIs and the nature of substituents remains uncertain in the SCIs oligomerization reactions.

In the present study, we mainly focus on the oligomerization reaction mechanisms and kinetics of four carbonyl oxides reactions with their hydroperoxide esters as well as with HPMF by employing quantum chemical calculations and kinetics modeling methods. For the initiation reactions of carbonyl oxides with formic acid, four kinds of pathways including 1,4 O-H insertion, 1,2 O-H insertion, C-H insertion, and C=O cycloaddition are considered. For the oligomerization reactions of the successive insertion of carbonyl oxides into hydroperoxide esters, two types of reactions involving –OOH and –CH insertions are taken into account. The selected carbonyl oxides, including CH_2OO, *syn*-, *anti*-CH_3CHOO and $(CH_3)_2CHOO$, are anticipated upon the ozonolysis of ethylene, propylene, and 2,3-dimethyl-2-butene, whereas the hydroperoxide esters are assumed to arise from the bimolecular reactions of carbonyl oxides with formic acid in the atmosphere.

2. Computational details

2.1 Electronic structure and energy calculations

https://doi.org/10.5194/acp-2022-376
Preprint. Discussion started: 8 June 2022


Atmospheric Chemistry and Physics Discussions

All electronic structure calculations are carried out by using Gaussian 09 program (Frisch et al., 2009). The geometries of all stationary points, including reactants (R), intermediates (IM), transition states (TS), and products (P), are optimized at the M06-2X/6-311+G(2df,2p) level of theory, since the M06-2X functional has the reliable performance for predicting thermochemistry, kinetics and hydrogen bonding interactions (Zhao and Truhlar, 2008). Harmonic vibrational frequencies are performed at the same level to verify the nature of transition state (NIMAG = 1) and saddle point (NIMAG = 0), and to provide zero-point vibrational energy (ZPVE) and Gibbs free energies corrections (G_{corr}), which are scaled by a factor of 0.98 (Alecu et al., 2010). Intrinsic reaction coordinate (IRC) calculations are carried out to verify that each transition state is connected to the desired reactant and product (Fukui, 1981). The single point energy (SPE) calculations are performed at the M06-2X/ma-TZVP level of theory based on the M06-2X/6-311+G(2df,2p) optimized geometries. Moreover, the basis set superposition error (BSSE) is performed by using the counterpoise method proposed by Boys and Bernardi (1970) to evaluate the stability of pre-reactive complexes (RC). Herein, the Gibbs free energy (G) is defined as the sum of SPE and Gibbs correction ($G = E + G_{corr}$). Electronic energy ($\Delta E^{\neq}$) and Gibbs free energy ($\Delta G^{\neq}$) barriers are defined as the difference in energy between a TS and a RC ($\Delta E^{\neq} = E_{TS} - E_{RC}$ and $\Delta G^{\neq} = G_{TS} - G_{RC}$). Reaction Gibbs free energy (ΔG) is defined as the difference in energy between a P and a R ($\Delta G = G_P - G_R$).

To further assess the reliability of the selected M06-2X/ma-TZVP method for SPE calculations, the single point energies of all stationary points involved in the initiation reactions of distinct SCIs with HCOOH are recalculated at the high-precision CCSD(T)/6-311+G(2df,2p) and QCISD(T)/6-311+G(2df,2p) levels of theory. The calculated results are summarized in Table S1. This table shows that the $\Delta E^{\neq}$ and $\Delta G^{\neq}$ obtained using the QCISD(T) method are in excellent agreement with those obtained using the CCSD(T) approach. It is therefore that the energies obtained using the CCSD(T) method are used as the benchmark for comparation. The mean

https://doi.org/10.5194/acp-2022-376
Preprint. Discussion started: 8 June 2022

Atmospheric Chemistry and Physics Discussions

absolute deviations (MAD) of $\Delta E^{\neq}$ and $\Delta G^{\neq}$ between the CCSD(T) and M06-2X methods are 0.43 and 0.41 kcal mol^{-1}, respectively; the largest deviations of $\Delta E^{\neq}$ and $\Delta G^{\neq}$ are 1.0 and 1.1 kcal mol^{-1}, respectively. These results reveals that the energies obtained using the M06-2X method are close to those obtained using the CCSD(T) approach. Therefore, the M06-2X/ma-TZVP method is suitable to investigate the SCIs oligomerization reactions. In the following discussion, the energies are applied in terms of Gibbs free energy to describe the reaction mechanism unless otherwise stated.

2.2 Kinetics calculations

The rate coefficients for the barrierless reactions are determined by employing the variational transition state theory (VTST) (Georgievskii and Klippenstein, 2005), and the rate coefficients for tight transition states are calculated by using the canonical transition state theory (CTST) along with one-dimensional asymmetric Eckart tunneling correction (Truhlar, et al., 1996; Eckart, 1930). As shown in Fig. 1, the entrance pathway Entry2 of R_1R_2COO reactions with HCOOH consists of two steps: (i) an intermediate IMent2 is formed via a barrierless process; (ii) then, it decomposes to the product Pent2 through a tight transition state TSent2. The whole reaction process can be described as Eq. (1):

$$R_1R_2COO + HCOOH \underset{k_{-1}}{\overset{k_1}{\rightleftharpoons}} IMent2 \xrightarrow{k_2} Pent2 \quad (1)$$

Assuming the rapid equilibrium is established between IMent2 and reactants. According to the steady-state approximation (SSA), the total rate coefficient is approximately expressed as Eq. (2) (Zhang et al., 2012):

$$k_{tot} = \frac{k_1}{k_{-1} + k_2} k_2 \approx \frac{k_1}{k_{-1}} k_2 = K_{eq} k_2 \quad (2)$$

The equilibrium constant K_{eq} is written as Eq. (3):

$$K_{eq} = \sigma \frac{Q_{IM}(T)}{Q_{R1}(T) Q_{R2}(T)} \exp\left(\frac{G_R - G_{IM}}{RT}\right) \quad (3)$$

where σ refers to reaction symmetry number, $Q_{IM}(T)$, $Q_{R1}(T)$ and $Q_{R2}(T)$ denote

https://doi.org/10.5194/acp-2022-376
Preprint. Discussion started: 8 June 2022


Atmospheric Chemistry and Physics Discussions

the partition functions of intermediate, reactants R1 and R2, which are equal to the multiplication of translational, rotational, vibrational and electronic partition functions ($Q = Q_{rot}Q_{vib}Q_{trans}Q_{elec}$) (Mendes et al., 2014), T is the temperature in Kelvin, R is the ideal gas constant, G_R and G_{IM} are the total Gibbs free energies of reactant and intermediate, respectively. The kinetic calculations are performed by utilizing the KiSThelP 2019 program (Canneaux et al., 2013).

3. Results and discussion

3.1 Initiation reactions of distinct SCIs with HCOOH

The reaction with HCOOH is one of the dominant loss processes for SCIs and is expected to trigger the formation of SOA in the atmosphere (Chhantyal-Pun et al., 2018; Cabezas and Endo, 2020; Zhao et al., 2018; Zhou et al., 2019). The potential energy surface (PES) of distinct SCIs (CH_2OO, *syn*-, *anti*-CH_3CHOO and $(CH_3)_2COO$) reactions with HCOOH is drawn in Fig. 1. The geometries of all stationary points are displayed in Fig. S1. The relative free energy of each stationary point and free energy barrier ($\Delta G^{\neq}$) of each elementary reaction are summarized in Table 1. As shown in Fig. 1, the bimolecular reaction of distinct SCIs with HCOOH proceeds via four possible pathways, namely (1) 1,4 O-H insertion (Entry 1), (2) 1,2 O-H insertion (Entry 2), (3) C-H insertion (Entry 3), and (4) C=O cycloaddition (Entry 4). For Entry 1, the addition reactions proceed through the barrierless 1,4 O-H insertion of carbonyl oxides into HCOOH to form hydroperoxide esters Pent1 with exoergicities of > 25 kcal mol^{-1}. Despite an attempt by various methods, the corresponding transition state is still not located in the effort of optimization. This conclusion is further supported by the analogous reaction systems that 1,4 O-H insertion reaction is a barrierless process (Long et al., 2009; Vereecken, 2017; Cabezas and Endo, 2019; Lin et al., 2019). The detailed mechanism includes that the O=C-OH moiety of HCOOH connects to the center carbon of SCIs, while the remaining hydrogen atom transfers to the terminal oxygen of SCIs resulting in the formation of Pent1. The exothermicity of different pathways decreases in the order of 37.6 (CH_2OO) > 34.0 (*anti*-CH_3CHOO) > 29.8 (*syn*-CH_3CHOO) > 25.6 ($(CH_3)_2COO$) kcal mol^{-1}, indicating that the

https://doi.org/10.5194/acp-2022-376
Preprint. Discussion started: 8 June 2022


Atmospheric Chemistry and Physics Discussions

exothermicity is highly dependent on the number and location of methyl groups. For example, the exothermicity of the parent CH_2OO + HCOOH reaction is the largest, whereas it becomes the smallest when two methyl groups are introduced at the R_1 and R_2 positions of CH_2OO. The exothermicity of *anti*-CH_3CHOO + HCOOH reaction is about 4.0 kcal mol^{-1} higher than that of *syn*-CH_3CHOO + HCOOH system.

For Entry 2, each addition reaction starts with the formation of a pre-reactive hydrogen bonded complex IMent2 in the entrance channel. Then it immediately converts into product Pent2 through the respective transition state. The reaction mechanism involves that the HCOO– fragment of HCOOH binds to the center carbon of SCIs, whereas the remnant –H fragment adds to the SCIs terminal oxygen resulting in the formation of Pent2. The reaction barrier $\Delta G^{\neq}$ increases in the order of 10.0 (CH_2OO) < 13.0 (*anti*-CH_3CHOO) < 14.6 (*syn*-CH_3CHOO) ≈ 14.4 ($(CH_3)_2COO$) kcal mol^{-1}, suggesting that the parent CH_2OO + HCOOH reaction is favored kinetically. Compared with the barrier of parent system, the barrier increases by 3.0 kcal mol^{-1} when methyl substitution occurs at the R_1 position, and the barrier increases by ~ 5 kcal mol^{-1} when the methyl groups are introduced at the R_2 position and R_1 and R_2 positions. The aforementioned result implies that the methyl-substituted CH_2OO hinders the 1,2 O-H insertion of carbonyl oxides into formic acid. Notably, the exothermicity decreases significantly as the number of methyl group is increased. The products Pent1 and Pent2 formed from Entry 1 and 2 are two conformations that differ in the orientation of the –C(O)H moiety over the –OOH group. The calculated result shows that Pent1 is more stable than Pent2 in energy due to the existence of intramolecular hydrogen bond between hydrogen atom of –OOH group and carbonyl oxygen atom.

For Entry 3, the addition reaction begins with the formation of a pre-reactive complex IMent3 in the entrance channel, and then it surmounts a barrier to reaction. However, the barriers of C-H insertion reactions are high (21.8-27.6 kcal mol^{-1}), such that they are of less importance in the atmosphere. The high reaction barriers might be attributed to the large bond dissociation energy (BDE) of C-H bond in the formic acid. For Entry 4, the addition reaction proceeds through the cycloaddition of SCIs to the

https://doi.org/10.5194/acp-2022-376
Preprint. Discussion started: 8 June 2022


Atmospheric Chemistry and Physics Discussions

C=O bond of HCOOH to produce a five-membered ring compound Pent4. The barrier of C=O cycloaddition reaction in the CH_2OO + HCOOH reaction is 5.8 kcal mol^{-1}, which is lower than that of the corresponding channels in Entry 2 and Entry 3 by 4.2 and 16.0 kcal mol^{-1}, respectively. The result reveals that the C=O cycloaddition reaction is feasible kinetically. A similar conclusion is also obtained from the reactions of HCOOH with *syn*-/*anti*-CH_3CHOO and $(CH_3)_2COO$ that the C=O cycloaddition reactions are favored over 1,2 O-H and C-H insertion reactions.

The rate coefficients of each elementary pathway are calculated in the temperature range of 273-400 K as listed in Table S2-S5. As shown in Table S2, the total rate coefficients k_{tot} of CH_2OO reaction with HCOOH are as high as ~ 10^{-10} cm^3 $molecule^{-1}$ s^{-1} and exhibit a slightly negative temperature dependence in the temperature range studied. At room temperature, k_{tot} is estimated to be 3.6×10^{-10} cm^3 $molecule^{-1}$ s^{-1}, which is greater by a factor of ~3 than that reported by Welz et al. (2014) ($[1.1 \pm 0.1] \times 10^{-10}$ cm^3 $molecule^{-1}$ s^{-1}), Chung et al. (2019) ($[1.4 \pm 0.3] \times 10^{-10}$ cm^3 $molecule^{-1}$ s^{-1}), and Peltola et al. (2020) ($[1.0 \pm 0.03] \times 10^{-10}$ cm^3 $molecule^{-1}$ s^{-1}). k(TSent1) is approximately equal to k_{tot} in the whole temperature range, and it decreases in the range of 4.3×10^{-10} (273 K) to 2.1×10^{-10} (400 K) cm^3 $molecule^{-1}$ s^{-1} with increasing temperature. k(TSent1) is several orders of magnitude greater than k(TSent2), k(TSent3) and k(TSent4) over the temperature range from 273 to 400 K. The result again shows that the barrierless 1,4 O-H insertion reaction is predominant. It should be noted that although the barrier of Entry 2 is 4.2 kcal mol^{-1} higher than that of Entry 4, the rate coefficient k(TSent2) is merely about 1-2 fold smaller than k(TSent4). The reason is ascribed to the fact that the C=O cycloaddition reaction is entropically unfavorable (Vereecken, 2017).

Entry 2 is competitive with Entry 4 in the *anti*-CH_3CHOO + HCOOH reaction (Table S3), while the competition of Entry 2 is significantly greater than that of Entry 4 in the *syn*-CH_3CHOO + HCOOH and $(CH_3)_2COO$ + HCOOH systems (Table S4-S5). This result shows that the relative importance of different pathways is highly dependent on the number and location of methyl substituents in the carbonyl oxides. Notably, the rate coefficient of each elementary pathway included in the

https://doi.org/10.5194/acp-2022-376
Preprint. Discussion started: 8 June 2022

Atmospheric Chemistry and Physics Discussions

anti-CH_3CHOO + HCOOH reaction is several orders of magnitude greater than that of the corresponding channel involved in the other SCIs + HCOOH systems. It is because that *anti*-CH_3CHOO is substantially more reactive toward HCOOH than other SCIs. Similar phenomenon has also observed from the reactivity of *anti*-CH_3CHOO toward water and SO_2 (Taatjes, et al., 2013; Long et al., 2016; Huang et al., 2015; Cabezas and Endo, 2018). At ambient temperature, the total rate coefficients of HCOOH reactions with *syn*-CH_3CHOO, *anti*-CH_3CHOO and $(CH_3)_2COO$ are estimated to be 9.8, 7.2 and 5.4 × 10^{-10} cm^3 $molecule^{-1}$ s^{-1}, respectively, which are in good agreement with the prior experimental measurements 5 ± 3, 2.5 ± 0.3 and 4.5 × 10^{-10} cm^3 $molecule^{-1}$ s^{-1} (Welz et al., 2014; Chung et al., 2019; Sipilä et al., 2014).

Based on the aforementioned discussions, it can be concluded that the barrierless 1,4 O-H insertion reaction is the dominant pathway in the initiation reactions of distinct SCIs with HCOOH. This conclusion is consistent with the recent experimental results derived from the reactions of formic acid with methacrolein oxide (MACR-oxide) and methyl vinyl ketone oxide (MVK-oxide) that the 1,4-addition mechanism is energetically favorable (Vansco et al., 2021; Caravan et al., 2020). Therefore, in the present study, the products Pent1 formed form the barrierless 1,4 O-H insertion of carbonyl oxides into HCOOH are selected as the model compounds to investigate the oligomerization reaction mechanisms of carbonyl oxides reactions with hydroperoxide esters.

https://doi.org/10.5194/acp-2022-376
Preprint. Discussion started: 8 June 2022

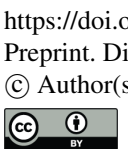

Atmospheric Chemistry and Physics Discussions

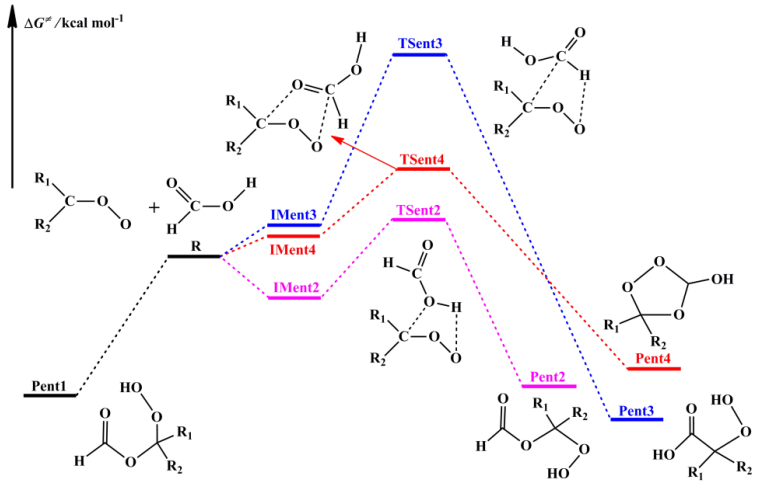

Figure 1. Schematic PES for the possible entrance pathways of the initiation reactions of SCIs with HCOOH (black, pink, blue, and red lines represent 1,4 O-H insertion, 1,2 O-H insertion, C-H insertion, and C=O cycloaddition reactions, respectively)

Table 1 Relative free energies of stationary points and free-energy barriers ($\Delta G^{\neq}$) at 298 K in kcal mol^{-1} for the various SCIs (R_1R_2COO, R_1, R_2=H, CH_3) reactions with HCOOH calculated at the M06-2X/ma-TZVP//M06-2X/6-311+G(2df,2p) level of theory

Entry	R1	R2	IMent	TSent	Pent	$\Delta G^{\neq}$
1	H	H	–	–	-37.6	–
	CH_3	H	–	–	-34.0	–
	H	CH_3	–	–	-29.8	–
	CH_3	CH_3	–	–	-25.6	–
2	H	H	-3.1	6.9	-37.3	10.0
	CH_3	H	-11.0	2.0	-33.7	13.0
	H	CH_3	-6.6	8.0	-29.1	14.6
	CH_3	CH_3	-8.8	5.6	-24.9	14.4
3	H	H	3.4	25.2	-46.9	21.8
	CH_3	H	1.8	24.0	-41.5	22.2
	H	CH_3	3.0	30.6	-37.6	27.6
	CH_3	CH_3	1.9	29.5	-33.0	27.6
4	H	H	3.4	9.2	-31.7	5.8
	CH_3	H	2.2	7.8	-29.4	5.6
	H	CH_3	3.5	14.6	-25.3	11.1
	CH_3	CH_3	3.0	13.2	-22.9	10.2

3.2 The reactions of distinct SCIs with their respective hydroperoxide esters

https://doi.org/10.5194/acp-2022-376
Preprint. Discussion started: 8 June 2022


Atmospheric Chemistry and Physics Discussions

The formed hydroperoxide ester has two possible unimolecular decomposition pathways. The first is the direct O-O bond rupture resulting in the formation of oxylmethylformate and OH radicals (Vereecken, 2017). The second is the –OH fragment binding to adjacent hydrogen atom leading to the formation of anhydride and H_2O (Aplincourt and Ruiz-López, 2000; Neeb et al., 1998). However, the barriers of these two unimolecular reactions are extremely high, such that they are of less importance in the atmosphere. The formed hydroperoxide ester possess –OOH and –OC(O)H groups, both of them can serve as the reactive moieties to react with carbonyl oxides giving rise to the formation of oligomers. In the present study, we mainly consider two types of pathways: (a) –OOH insertion and (b) –CH insertion, while the C=O cycloaddition reaction is not taken into account because it is entropically unfavorable (Vereecken, 2017; Lin et al., 2019). The aforementioned reactions are discussed in detail in the following subsections.

3.2.1 The reactions of $2CH_2OO$ with Pent1a

The simplest carbonyl oxide, CH_2OO, originates from the reaction of all terminal alkenes with ozone (ozonolysis) in the atmosphere (Lin and Chao, 2017). The reaction with HCOOH is expected to be one of the dominant loss processes for CH_2OO, and the main product is HPMF (Welz et al., 2014; Cabezas and Endo, 2019). The schematic PES for the addition reaction $2CH_2OO$ + Pent1a (HPMF) is drawn in Fig. 2, and the optimized geometries of all stationary points are displayed in Fig. S2. As seen from Fig. 2, the successive insertion of CH_2OO into Pent1a eventually leads to the formation of oligomers P2a and P2b composed of CH_2OO as the repeat unit. These oligomerization reactions are strongly exothermic and spontaneous (> 83 kcal·mol^{-1}), implying that they are feasible thermodynamically. For the initial –OOH insertion reaction R1a, the pre-reactive intermediate IM1a with a seven-membered ring structure is formed, which is stabilized by the hydrogen bond interactions between the H_4 atom of Pent1a and the O_6 atom of CH_2OO ($D_{(O6\text{-}H4)}$ = 1.706 Å), and between the H_6 atom of CH_2OO and the O_3 atom of Pent1a ($D_{(O3\text{-}H6)}$ = 2.115 Å). Then it converts into P1a ($C_3H_6O_6$, HC(O)O–$(CH_2OO)_2$–H) with a barrier of 8.1 kcal·mol^{-1} and an

https://doi.org/10.5194/acp-2022-376
Preprint. Discussion started: 8 June 2022


Atmospheric Chemistry and Physics Discussions

exoergicity of 40.4 kcal mol^{-1}. The reaction mechanism involves that the –$OOCH_2OC(O)H$ fragment of Pent1a connects to the C_3 atom of CH_2OO, while the remaining H_4 atom binds to the CH_2OO terminal O_6 atom. For the initial –CH insertion reaction R1b, a weakly hydrogen bonded intermediate IM1b is formed in the entrance channel, then it transforms into P1b ($C_3H_6O_6$, $HO_2CH_2OC(O)CH_2OOH$) with a barrier of 21.5 kcal mol^{-1}. The detailed mechanism includes that the $HOOCH_2OC(O)$– fragment of Pent1a binds to the C_3 atom of CH_2OO, while the remnant H_1 atom adds to the terminal O_6 atom of CH_2OO. The barrier of R1b is higher than that of R1a by 13.4 kcal mol^{-1}, suggesting that the –OOH insertion reaction is favorable energetically.

Equivalent to the reaction of CH_2OO with Pent1a, the addition reaction between CH_2OO and P1a starts with the formation of cyclic intermediates IM2a and IM2b in the entrance channel. The relative energies of IM2a and IM2b with respect to the separate reactants P1a and CH_2OO are -1.2 and 3.2 kcal mol^{-1}, respectively, below the energies of the initial reactants $2CH_2OO$ and Pent1a are 41.6 and 37.2 kcal mol^{-1}, respectively. Then they immediately transform into the respective products P2a and P2b via the –OOH and –CH insertion transition states TS2a and TS2b with the barriers of 10.1 and 21.6 kcal mol^{-1}. This result again shows that the –OOH insertion reaction is favored over the –CH insertion pathway. This result is consistent with the prior previous study that –CH insertion reaction is of minor importance in the bimolecular reaction of CH_2OO with alkenes (Buras et al., 2014). It deserves mentioning that the barrier of –OOH insertion reaction increases as the number of CH_2OO is increased.

https://doi.org/10.5194/acp-2022-376
Preprint. Discussion started: 8 June 2022

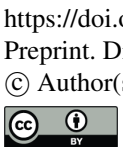

Atmospheric Chemistry and Physics Discussions

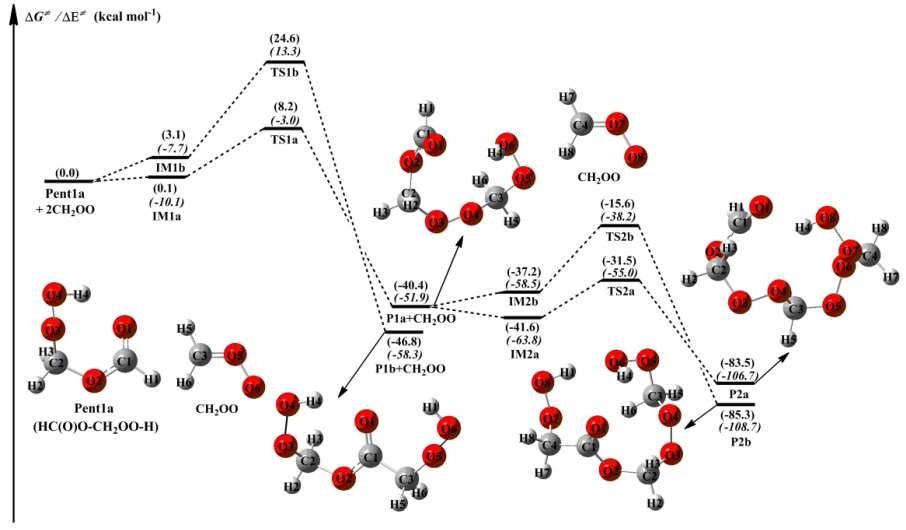

Figure 2. PES (ΔG and ΔE, in italics) for the $2CH_2OO$ + Pent1a reaction at the M06-2X/ma-TZVP//M06-2X/6-311+G(2df,2p) level of theory.

3.2.2 The reactions of *anti*-CH_3CHOO with Pent1b

The methyl-substituted CH_2OO has two conformers, *syn*- and *anti*-CH_3CHOO that distinguish by the orientation of methyl group relative to the terminal oxygen (Taatjes et al., 2013). *syn*-CH_3CHOO is more stable than *anti*-CH_3CHOO in energy due to the existence of intermolecular hydrogen bond (Long et al., 2016). The activation enthalpy of the interconversion between *syn*-CH_3CHOO and *anti*-CH_3CHOO is up to 38.5 kcal mol^{-1}, implying that they can treat as independent species in the atmosphere (Long et al., 2016; Yin and Takahashi, 2017). The schematic PES for the addition reaction 2*anti*-CH_3CHOO + Pent1b is presented in Fig. 3, and the optimized geometries of all stationary points are shown in Fig. S3. As shown in Fig. 3, the addition reaction 2*anti*-CH_3CHOO + Pent1b proceeds through successive insertion of *anti*-CH_3CHOO into Pent1b leading to the formation of oligomers P4a and P4b that contain *anti*-CH_3CHOO as chain unit. The first *anti*-CH_3CHOO addition reaction begins with the formation of IM3a and IM3b in the entrance channel, which lie -2.2 and 2.4 kcal mol^{-1} respectively, with respect to the separate reactants. Then the IM3a and IM3b transform into P3a and P3b via –OOH and –CH insertion transition states TS3a and TS3b with the barriers of 5.6 and 20.3

https://doi.org/10.5194/acp-2022-376
Preprint. Discussion started: 8 June 2022

Atmospheric Chemistry and Physics Discussions

kcal mol^{-1}. This result shows that the –OOH insertion reaction is more favorable than the –CH insertion pathway. Compared with the barriers of R1a and R1b in the 2CH_2OO + Pent1a reaction, the barriers of R3a and R3b decrease by 2.5 and 1.2 kcal mol^{-1} when a methyl group is introduced at the *anti*-position. The result reveals that the reactivity of *anti*-CH_3CHOO is substantially higher than that of CH_2OO. This conclusion is further supported by the findings of other studies, which have reported that *anti*-CH_3CHOO is more reactive toward H_2O, SO_2, and H_2O_2 than CH_2OO (Chen et al., 2017; Taatjes et al., 2013; Huang et al., 2015). Similarly, the secondary *anti*-CH_3CHOO addition reaction starts with the formation of IM4a and IM4b in the entrance channel with the 0.1 and 3.7 kcal mol^{-1} stability, followed by conversion to the final products P4a and P4b through the –OOH and –CH insertion reactions R4a and R4b. The transition states TS4a and TS4b lie 7.0 and 21.0 kcal mol^{-1}, respectively, above the energies of the respective intermediates IM4a and IM4b. This result again shows that the –OOH insertion reaction is the most favorable channel, and the barrier increases as the number of *anti*-CH_3CHOO is increased. This conclusion is consistent with the result obtained from the 2CH_2OO + Pent1a reaction that the first CH_2OO addition reaction is favored energetically.

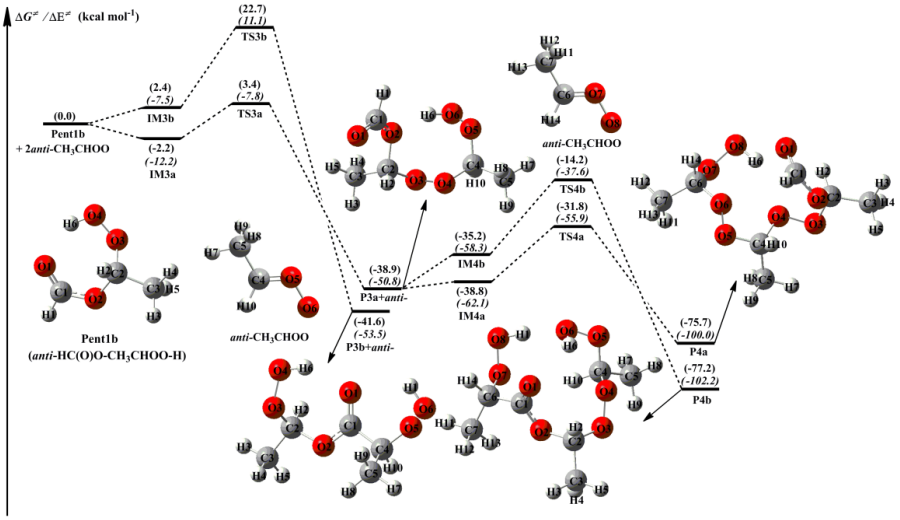

Figure 3. PES (Δ*G* and Δ*E*, in italics) for the 2*anti*-CH_3CHOO + Pent1b reaction at the M06-2X/ma-TZVP//M06-2X/6-311+G(2df,2p) level of theory

https://doi.org/10.5194/acp-2022-376
Preprint. Discussion started: 8 June 2022


Atmospheric Chemistry and Physics Discussions

3.2.3 The reactions of *syn*-CH_3CHOO with Pent1c

Equivalent to the 2*anti*-CH_3CHOO + Pent1b reaction, the addition reaction 2*syn*-CH_3CHOO + Pent1c has similar transformation pathways, and is thus briefly discussed in the present study. From Fig. 4, it can be seen that the addition reaction 2*syn*-CH_3CHOO + Pent1c undergoes via successive insertion of *syn*-CH_3CHOO into Pent1c to form P6a and P6b that involve *syn*-CH_3CHOO as the repeating unit. The most favorable pathway is that the breakage of –OOH bond in Pent1c occurs simultaneously with the insertion of first *syn*-CH_3CHOO to form P5a, followed by the insertion of secondary *syn*-CH_3CHOO to produce P6a. The barriers of these two –OOH insertion reactions R5a and R6a are 13.8 and 11.8 kcal·mol^{-1}, respectively, which are higher than those of R3a and R4a in the 2*anti*-CH_3CHOO + Pent1b system by 8.2 and 4.8 kcal·mol^{-1}, respectively. The result reveals that the reactivity of *syn*-CH_3CHOO is substantially lower than that of *anti*-CH_3CHOO. The reactivity of *anti*- and *syn*-CH_3CHOO can be attributed to the total contributions of electrostatic and steric hindrance effects, in which steric hindrance is obviously dominant for *syn*-CH_3CHOO, that is not thus conducive to the nucleophilic attack of hydroperoxide esters. Notably, the barrier of the favorable –OOH insertion pathway decreases with increasing the number of *syn*-CH_3CHOO in the 2*syn*-CH_3CHOO + Pent1c reaction, which is contrary to the case of the $2CH_2OO$ + Pent1a and 2*anti*-CH_3CHOO + Pent1b reactions.

https://doi.org/10.5194/acp-2022-376
Preprint. Discussion started: 8 June 2022

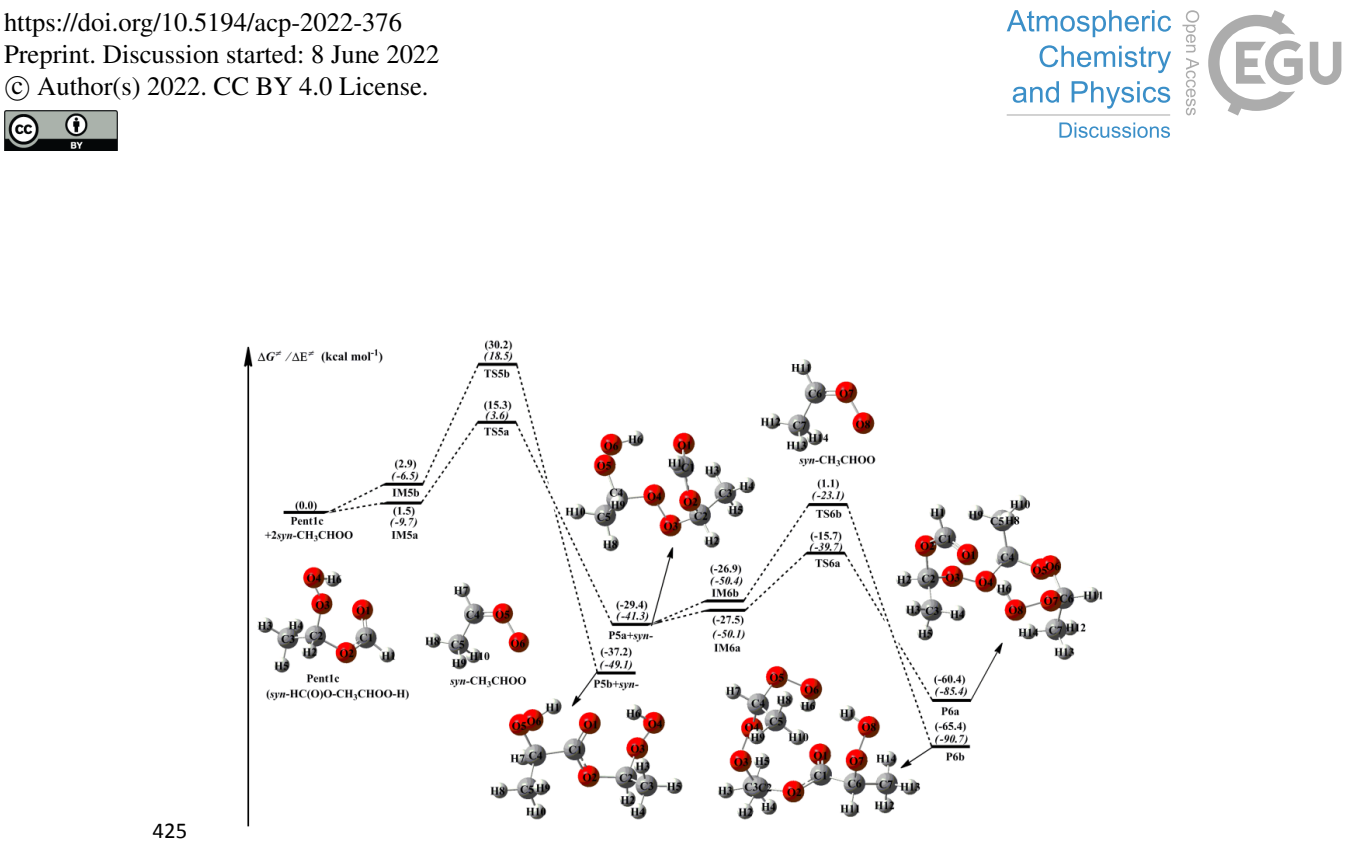

Figure 4. PES (Δ*G* and Δ*E*, in italics) for the 2*syn*-CH_3CHOO + Pent1c reaction at the M06-2X/ma-TZVP//M06-2X/6-311+G(2df,2p) level of theory

3.2.4 The reactions of 2$(CH_3)_2COO$ with Pent1d

The dimethyl-substituted Criegee intermediate, $(CH_3)_2COO$, is generated from the ozonolysis of 2,3-dimethyl-2-butene in the atmosphere (Lester and Klippenstein, 2018; Drozd et al., 2017; Long et al., 2018). The bimolecular reaction of $(CH_3)_2COO$ with water is not fast enough ($k < 1.5 \times 10^{-16}$ cm^3 molecule^{-1} s^{-1}), while the reaction of $(CH_3)_2COO$ with HCOOH has a near gas kinetic limit rate ($k = 5.4 \times 10^{-10}$ cm^3 molecule^{-1} s^{-1}) (Huang et al., 2015). The result implies that a fraction of $(CH_3)_2COO$ may survive under high humidity environments and react with HCOOH leading to the formation of hydroperoxide ester Pent1d. The schematic PES for the addition reaction 2$(CH_3)_2COO$ + Pent1d is plotted in Fig. 5, and the optimized geometries of all stationary points are shown in Fig. S5.

As can be seen in Fig. 5, the addition reaction 2$(CH_3)_2COO$ + Pent1d starts with the formation of complexes IM7a and IM7b, which lie 1.9 and 2.4 kcal mol^{-1}, respectively, above the energies of the separate reactants. Then they subsequently transform into products P7a and P7b through the –OOH and –CH insertion transition states TS7a and TS7b with the barriers of 12.2 and 26.4 kcal mol^{-1}. This result again shows that the –OOH insertion reaction is favored over the –CH insertion pathway. A similar conclusion is also obtained from the secondary $(CH_3)_2COO$ addition reaction

https://doi.org/10.5194/acp-2022-376
Preprint. Discussion started: 8 June 2022

Atmospheric Chemistry and Physics Discussions

that the –OOH insertion reaction is the dominant pathway. It is of interest to compare the barriers of –OOH insertion reactions in the $(CH_3)_2COO$ + Pent1d system with those of the analogous reactions in other SCIs + Pent1 reactions. It can be found that the barriers decrease in the order of *syn*-CH_3CHOO > $(CH_3)_2COO$ > CH_2OO > *anti*-CH_3CHOO in the first-step SCIs addition reaction, while they become $(CH_3)_2COO$ > *syn*-CH_3CHOO > CH_2OO > *anti*-CH_3CHOO in the second-step SCI addition pathway. The result shows that the reactivity of SCIs is significantly affected by the number and location of methyl substituents. A similar conclusion is also obtained from the thermodynamic parameters that the exothermicity of –OOH insertion reactions significantly decreases with increasing the number of methyl substituents, and the exothermicity of *anti*-methyl substituted carbonyl oxide is obviously higher than that of *syn*-methyl substituted carbonyl oxide.

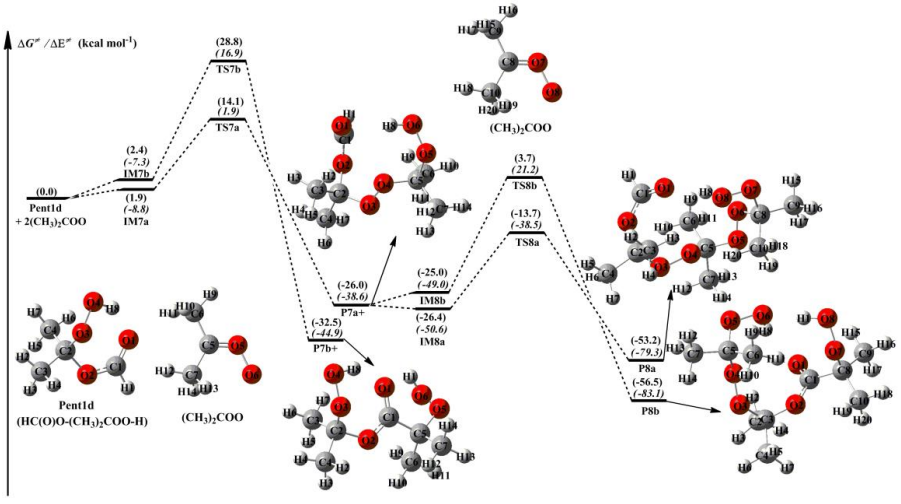

Figure 5. PES (Δ*G* and Δ*E*, in italics) for the 2$(CH_3)_2COO$ + Pent1d reaction at the M06-2X/ma-TZVP//M06-2X/6-311+G(2df,2p) level of theory.

3.3 The reactions of distinct SCIs with Pent1a

To further elucidate the effect of the number and location of methyl substituents on the reactivity of carbonyl oxides toward hydroperoxide esters, Pent1a is selected as the model compound since it is the simplest hydroperoxide ester formed from the barrierless 1,4 O-H insertion of CH_2OO into HCOOH. On the basis of aforementioned discussions, –OOH insertion reaction is the most favorable pathway. Therefore, this

https://doi.org/10.5194/acp-2022-376
Preprint. Discussion started: 8 June 2022


Atmospheric Chemistry and Physics Discussions

type of reaction is taken into consideration in the reactions of dictinct SCIs with Pent1a. The corresponding PES and the optimized geometries of all stationary points are displayed in Fig. 6 and S6, respectively. From Fig. 6, it is seen that the mechanism of Pent1a reactions with *anti*-CH_3CHOO, *syn*-CH_3CHOO and $(CH_3)_2COO$ is similar to that of the reaction CH_2OO + Pent1a discussed above. For each additon reaction, a pre-reactive intermediate is formed prior to the corresponding transition state, and then it overcomes a modest barrier to produce the respective product. Compared with the barrier of CH_2OO reaction with Pent1a (8.1 kcal·mol^{-1}), the barrier decreases by 2.5 kcal·mol^{-1} when a methyl substituent occurs at the *anti*-position, while the barrier increases by about 3.0 kcal·mol^{-1} when a methyl group is introduced at the *syn*-position and dimethyl substitutions. This result indicates that the reactivity of *anti*-CH_3CHOO is substantially higher than that of CH_2OO, *syn*-CH_3CHOO and $(CH_3)_2COO$. It is worth noting that the exothermicity of distinct SCIs reactions with Pent1a obviously decreases as the number of methyl group is increased, and the exothermicity of *anti*-methyl substituent is higher than that of *syn*-methyl substituent. As a result, the barrier heights and thermodynamic parameters of the oligomerization reactions of SCIs with hydroperoxide esters are significantly affected by the number and location of methyl substituents.

The rate coefficients of distinct SCIs reactions with Pent1a are calculated in the temperature range of 273-400 K as summarized in Table 2. As shown in Table 2, the rate coefficients k_{R1a} of the reaction CH_2OO + Pent1a decrease in the range of 5.0×10^{-11} (273 K) to 5.0×10^{-12} cm^3 molecule^{-1} s^{-1} (400 K) with increasing temperature. A similar phenomenon is also observed from the rate coefficients of Pent1a reactions with *anti*-CH_3CHOO (R9), *syn*-CH_3CHOO (R10), and $(CH_3)_2COO$ (R11) that they exhibit a slightly netative temperature dependence. k_{R9} is several orders of magnitude greater than k_{R1a}, k_{R10} and k_{R11} in the whole temperature range, suggesting that the bimolecular reaction *anti*-CH_3CHOO + Pent1a (R9) is favored kinetically. Compared with the rate coefficients of parent reaction R1a, the rate coefficients increase by about one order of magnitude when a methyl substituent occurs at the *anti*-position, whereas the rate coefficients decrease by 1-2 orders of magnitude when a methyl

https://doi.org/10.5194/acp-2022-376
Preprint. Discussion started: 8 June 2022


Atmospheric Chemistry and Physics Discussions

group is introduced at the *syn*-position. k_{R11} is greater than k_{R1a} by a factor of ~1.2 in the temperature range studied. It should be noted that although the barrier of R10 is nearly identical to that of R11, k_{R10} is 1-2 orders of magnitude lower than k_{R11} in the entire temperature range. This is probably because the rate coefficients are mediated by pre-reactive intermediates that IM11 is more stable than IM10 in energy.

It is of interest to assess whether the reactions of distinct SCIs with HPMF can compete well with the losses to reactions with other trace species (e.g., H_2O, HCOOH and SO_2), because it is well known that the reactions with other trace species are expected to be the dominant chemical sinks for SCIs in the atmosphere (Taatjes et al., 2013; Long et al., 2016). For the reactions of CH_2OO with H_2O, HCOOH and SO_2, the experimental rate coefficients are determined to be 1.5×10^{-15}, 1.1×10^{-10}, and 3.9×10^{-11} cm^3 $molecule^{-1}$ s^{-1}, respectively (Welz et al., 2014; Huang et al., 2015; Chao et al., 2015). The atmosphereric concentrations of H_2O, HCOOH and SO_2 in forest environments are measured to be 3.9-6.1 $\times 10^{17}$, 5.0-10 $\times 10^{10}$, and 1.7-9.0 $\times 10^{10}$ molecules cm^{-3}, respectively (Vereecken et al., 2012). The effective rate coeffiient of CH_2OO reactions with H_2O ($k_{eff(H2O)}$), HCOOH ($k_{eff(HCOOH)}$) and SO_2 ($k_{eff(SO2)}$) are calculated to be 5.9-9.2 $\times 10^2$, 5.5-11, 0.7-3.5 s^{-1}, respectively. The result indicates that the CH_2OO + H_2O reaction is favored over bimolecular reactions with HCOOH and SO_2. Similar conclusion is also obtained from the reactions of other carbonyl oxides with H_2O, HCOOH and SO_2. Acconding to the results shown in the Table 2, the room temperature rate coefficient for the reaction of CH_2OO with HPMF is calculated to be 2.7×10^{-11} cm^3 $molecule^{-1}$ s^{-1}. However, to the best of our knowledge, the atmospheric concentration of HPMF has not been reported up to now. We assume the concentration of HPMF is the same as that of HCOOH in the atmosphere. The effective rate coefficient of CH_2OO reaction with HPMF ($k_{eff(HPMF)}$) is estimated to be 1.4-2.7 s^{-1}, which is significantly lower than $k_{eff(H2O)}$ and $k_{eff(HCOOH)}$. $k_{eff(HPMF)}$ is nearly identical to $k_{eff(SO2)}$. Based on the above discussions, it can be concluded that the reactions of carbonyl oxides with hydroperoxide esters play a certain role in the formation of organic new particle in some regions where low concentration of water vapor and high concentration of hydroperoxide esters occur.

https://doi.org/10.5194/acp-2022-376
Preprint. Discussion started: 8 June 2022

Atmospheric Chemistry and Physics Discussions

Table 2 The rate coefficients of distinct SCIs reactions with Pent1a computed at different temperatures

T/K	k_{CH2OO}(R1a)	$k_{anti\text{-}CH3CHOO}$(R9)	$k_{syn\text{-}CH3CHOO}$(R10)	$k_{(CH3)2COO}$(R11)
273	5.0×10^{-11}	6.4×10^{-10}	2.0×10^{-13}	4.4×10^{-11}
280	4.2×10^{-11}	4.7×10^{-10}	1.9×10^{-13}	3.5×10^{-11}
298	2.7×10^{-11}	3.3×10^{-10}	1.7×10^{-13}	2.2×10^{-11}
300	2.6×10^{-11}	2.8×10^{-10}	1.7×10^{-13}	2.1×10^{-11}
320	1.7×10^{-11}	2.3×10^{-10}	1.5×10^{-13}	1.4×10^{-11}
340	1.2×10^{-11}	1.7×10^{-10}	1.4×10^{-13}	9.4×10^{-12}
360	8.5×10^{-12}	1.1×10^{-10}	1.3×10^{-13}	6.9×10^{-12}
380	6.4×10^{-12}	8.3×10^{-11}	1.2×10^{-13}	5.3×10^{-12}
400	5.0×10^{-12}	5.3×10^{-11}	1.2×10^{-13}	4.2×10^{-12}

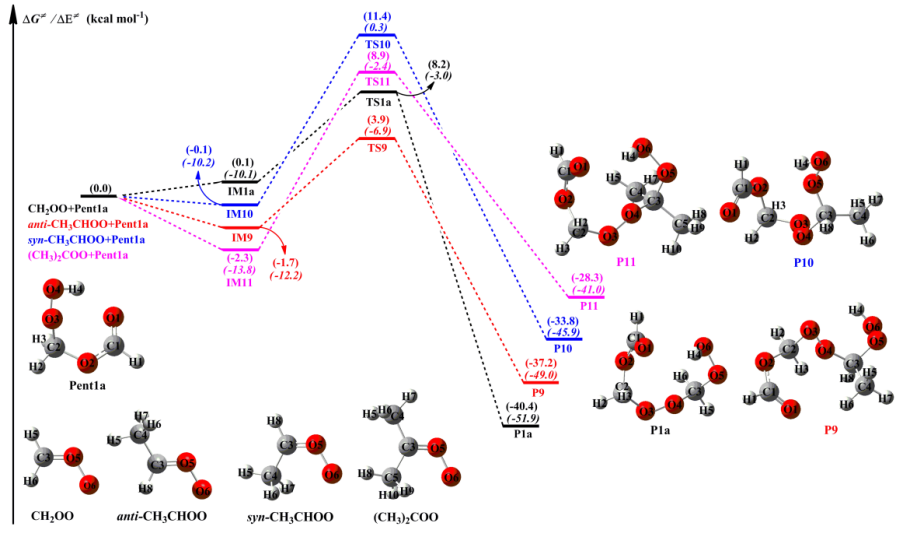

Figure 6. PES (ΔG and ΔE, in italics) for the distinct SCIs + Pent1a reactions at the M06-2X/ma-TZVP//M06-2X/6-311+G(2df,2p) level of theory

4. Conclusions

The oligomerization reaction mechanism and kinetics of Criegee intermediates reactions with their respective hydroperoxide esters as well as HPMF are investigated using quantum chemical calculations and kinetics modeling methods. The main conclusion is summarized as follows.

(a) For the initiation reactions of distinct SCIs with HCOOH, the barrierless 1,4

https://doi.org/10.5194/acp-2022-376
Preprint. Discussion started: 8 June 2022


Atmospheric Chemistry and Physics Discussions

O-H insertion reaction leading to the formation of hydroperoxide esters is the most favorable pathway. The exothermicity of the parent reaction CH_2OO + HCOOH is the largest, whereas it becomes the smallest when two methyl groups are introduced at the R_1 and R_2 positions of CH_2OO. The exothermicity of *anti*-CH_3CHOO + HCOOH reaction is about 4.0 kcal mol^{-1} higher than that of *syn*-CH_3CHOO + HCOOH system.

(b) The addition reactions of SCIs with hydroperoxide esters proceed through successive insertion of SCIs into hydroperoxide ester to form oligomers that involve SCIs as the repeating unit. These oligomerization reactions are strongly exthermoic and spontaneous. The exothermicity of oligomerization reactions significantly decreases when the number of methyl substituents increases, and the exothermicity of *anti*-methyl substituted carbonyl oxides is obviously higher than that of *syn*-methyl substituted carbonyl oxides.

(c) The –OOH insertion reaction is favored over the –CH insertion pathway in the SCIs oligomerization reactions, and the barrier heights increase with increasing the number of SCIs except *syn*-CH_3CHOO. The barrier of –OOH insertion pathway shows a dramatic decrease when a methyl substituent occurs at the *anti*-position, while it reveals a significant increase when a methyl group is introduced at the *syn*-position and dimethyl substitutions.

(d) Compared with the rate coefficients of the CH_2OO + HPMF reaction, the rate coefficients increase by about one order of magnitude when a methyl substituent occurs at the *anti*-position, whereas the rate coefficients decrease by 1-2 orders of magnitude when a methyl group is introduced at the *syn*-position.

Data availability

The data are accessible by contacting the corresponding author (huangyu@ieecas.cn).

Supplement

https://doi.org/10.5194/acp-2022-376
Preprint. Discussion started: 8 June 2022


Atmospheric Chemistry and Physics Discussions

566 The following information is provided in the Supplement: The electronic energy
567 ($\Delta E^{\neq}$) and Gibbs free energy ($\Delta G^{\neq}$) barriers for the initial reactions of distinct SCIs
568 with HCOOH predicted at different levels; Rate coefficients of initiation reactions of
569 distinct SCIs with HCOOH; Optimized geometries of all the stationary points.
570

571 ## Author contribution

572 LC designed the study. LC and YH wrote the paper. LC performed theoretical
573 calculation. YX, ZJ, and WW analyzed the data. All authors reviewed and commented
574 on the paper.
575

576 ## Competing interests

577 The authors declare that they have no conflict of interest.
578

579 ## Acknowledgments

580 This work was supported by the National Natural Science Foundation of China
581 (grant Nos. 42175134, 41805107, and 22002080). It was also partially supported as
582 Strategic Priority Research Program of the Chinese Academy of Sciences, China
583 (grant Nos. XDA23010300 and XDA23010000), and CAS "Light of West China"
584 Program (XAB2019B01).
585

586 ## References

587 Alecu, I. M., Zheng, J., Zhao, Y., and Truhlar, D. G.: Computational thermochemistry: scale factor
588 databases and scale factors for vibrational frequencies obtained from electronic model
589 chemistries, J. Chem. Theory Comput., 6, 2872-2887, https://doi.org/10.1021/ct100326h,
590 2010.
591 Anglada, J. M., and Solé, A.: Impact of the water dimer on the atmospheric reactivity of carbonyl
592 oxides, Phys. Chem. Chem. Phys., 18, 17698-17712, https://doi.org/10.1039/C6CP02531E,
593 2016.
594 Aplincourt, P., and Ruiz-López, M. F.: Theoretical study of formic acid anhydride formation from
595 carbonyl oxide in the atmosphere, J. Phys. Chem. A, 104, 380-388,
596 https://doi.org/10.1021/jp9928208, 2000.

https://doi.org/10.5194/acp-2022-376
Preprint. Discussion started: 8 June 2022

Atmospheric Chemistry and Physics Discussions

597 Atkinson, R., and Arey, J.: Atmospheric degradation of volatile organic compounds, Chem. Rev.,
598 103, 4605-4638, https://doi.org/10.1021/cr0206420, 2003.
599 Boys, S. F., and Bernardi, F.: The calculation of small molecular interactions by the differences of
600 separate total energies. Some procedures with reduced errors, Mol. Phys., 19, 553-566,
601 https://doi.org/10.1080/00268977000101561, 1970.
602 Buras, Z. J., Elsamra, R. M. I., Jalan, A., Middaugh, J. E., and Green, W. H.: Direct kinetic
603 measurements of reactions between the simplest Criegee intermediate CH_2OO and alkenes, J.
604 Phys. Chem. A, 118, 1997-2006, https://doi.org/10.1021/jp4118985, 2014.
605 Cabezas, C., and Endo, Y.: Observation of hydroperoxyethyl formate from the reaction between
606 the methyl Criegee intermediate and formic acid, Phys. Chem. Chem. Phys., 22, 446-454,
607 https://doi.org/10.1039/C9CP05030B, 2020.
608 Cabezas, C., and Endo, Y.: The Criegee intermediate-formic acid reaction explored by rotational
609 spectroscopy, Phys. Chem. Chem. Phys., 21, 18059-18064,
610 https://doi.org/10.1039/c9cp03001h, 2019.
611 Cabezas, C., and Endo, Y.: The reactivity of the Criegee intermediate CH_3CHOO with water
612 probed by FTMW spectroscopy, J. Chem. Phys., 148, 014308-014315,
613 https://doi.org/10.1063/1.5009033, 2018.
614 Canneaux, S., Bohr, F., and Henon, E.: KiSThelP: a program to predict thermodynamic properties
615 and rate constants from quantum chemistry results, J. Comput. Chem., 35, 82-93,
616 https://doi.org/10.1002/jcc.23470, 2013.
617 Caravan, R. L., Vansco, M. F., Au, K., Khan, M. A. H., Li, Y. L., Winiberg, F. A. F., Zuraski, K.,
618 Lin, Y. H., Chao, W., Trongsiriwat, N., Walsh, P. J., Osborn, D. L., Percival, C. J., Lin, J. J.
619 M., Shallcross, D. E., Sheps, L., Klippenstein, S. J., Taatjes, C. A., and Lester, M. I.: Direct
620 kinetic measurements and theoretical predictions of an isoprene-derived Criegee intermediate,
621 Proc. Natl. Acad. Sci. U.S.A., 117, 9733-9740, https://doi.org/10.1073/pnas.1916711117,
622 2020.
623 Chaliyakunnel, S., Millet, D. B., Wells, K. C., Cady-Pereira, K. E., and Shephard, M. W.: A large
624 underestimate of formic acid from tropical fires: constraints from space-borne measurements,
625 Environ. Sci. Technol., 50, 5631-5640, https://doi.org/10.1021/acs.est.5b06385, 2016.
626 Chao, W., Hsieh, J. T., Chang, C. H., and Lin, J. J. M.: Direct kinetic measurement of the reaction
627 of the simplest Criegee intermediate with water vapor, Science, 347, 751-754,
628 https://doi.org/10.1126/science.1261549, 2015.
629 Chen, L., Huang, Y., Xue, Y., Cao J., and Wang, W.: Effect of oligomerization reactions of Criegee
630 intermediate with organic acid/peroxy radical on secondary organic aerosol formation from
631 isoprene ozonolysis, Atmos. Environ., 187, 218-229,
632 https://doi.org/10.1016/j.atmosenv.2018.06.001, 2018.
633 Chen, L., Huang, Y., Xue, Y., Cao, J., and Wang, W.: Competition between HO_2 and H_2O_2
634 reactions with CH_2OO/*anti*-CH_3CHOO in the oligomer formation: a theoretical perspective, J.
635 Phys. Chem. A, 121, 6981-6991, https://doi.org/10.1021/acs.jpca.7b05951, 2017.
636 Chen, L., Huang, Y., Xue, Y., Shen, Z., Cao, J., and Wang, W.: Mechanistic and kinetics
637 investigations of oligomer formation from Criegee intermediate reactions with hydroxyalkyl
638 hydroperoxides, Atmos. Chem. Phys., 19, 4075-4091,
639 https://doi.org/10.5194/acp-19-4075-2019, 2019.
640 Chhantyal-Pun, R., McGillen, M. R., Beames, J. M., Khan, M. A. H., Percival, C. J., Shallcross, D.

https://doi.org/10.5194/acp-2022-376
Preprint. Discussion started: 8 June 2022

E., and Orr-Ewing, A. J.: Temperature Dependence of the Rates of Reaction of Trifluoracetic Acid with Criegee Intermediates, Angew. Chem. Int. Ed., 129, 9172-9175, https://doi.org/10.1002/anie.201703700, 2017.

Chhantyal-Pun, R., Rotavera, B., Mcgillen, M. R., Khan, M. A. H., Eskola, A. J., Caravan, R. L., Blacker, L., Tew, D. P., Osborn, D. L., Percival, C. J., Taatjes, C. A., Shallcross D. E., and Orr-Ewing, A. J.: Criegee intermediate reactions with carboxylic acids: a potential source of secondary organic aerosol in the atmosphere, ACS Earth Space Chem., 2, 833-842, https://doi.org/10.1021/acsearthspacechem.8b00069, 2018.

Chung, C. A., Su, J. W., and Lee, Y. P.: Detailed mechanism and kinetics of the reaction of Criegee intermediate CH_2OO with HCOOH investigated via infrared identification of conformers of hydroperoxymethyl formate and formic acid anhydride, Phys. Chem. Chem. Phys., 21, 21445-21455, https://doi.org/10.1039/c9cp04168k, 2019.

Criegee, R.: Mechanism of ozonolysis, Angew. Chem. Int. Ed. Engl., 14, 745-752, https://doi.org/10.1002/anie.197507451, 1975.

Drozd, G. T., Kurtén, T., Donahue, N. M., and Lester, M. I.: Unimolecular decay of the dimethyl-substituted Criegee intermediate in alkene ozonolysis: decay time scales and the importance of tunneling, J. Phys. Chem. A, 121, 6036-6045, https://doi.org/10.1021/acs.jpca.7b05495, 2017.

Eckart, C.: The penetration of a potential barrier by electrons, Phys. Rev., 35, 1303-1309, https://doi.org/10.1103/PhysRev.35.1303, 1930.

Frisch, M. J., Trucks, G. W., Schlegel, H. B., Scuseria, G. E., Robb, M. A., Cheeseman, J. R., Montgomery, J. A. Jr., Vreven, T., Kudin, K. N., Burant, J. C., Millam, J. M., Iyengar, S. S., Tomasi, J., Barone, V., Mennucci. B., Cossi, M., Scalmani, G., Rega, N., Petersson, G. A., Nakatsuji, H., Hada, M., Ehara, M., Toyota, K., Fukuda, R., Hasegawa, J., Ishida, M., Nakajima, T., Honda, Y., Kitao, O., Nakai, H., Klene, M., Li, X., Knox, J. E., Hratchian, H. P., Cross, J. B., Adamo, C., Jaramillo, J., Gomperts, R., Stratmann, R. E., Yazyev, O., Austin, A. J., Cammi, R., Pomelli, C., Ochterski, J. W., Ayala, P. Y., Morokuma, K., Voth, G. A., Salvador, P., Dannenberg, J. J., Zakrzewski, V. G., Dapprich, S., Daniels, A. D., Strain, M. C., Farkas, O., Malick, D. K., Rabuck, A. D., Raghavachari, K., Foresman, J. B., Ortiz, J. V., Cui, Q., Baboul, A. G., Clifford, S., Cioslowski, J., Stefanov, B. B., Liu, G., Liashenko, A., Piskorz, P., Komaromi, I., Martin, R. L., Fox, D. J., Keith, T., Al-Laham, M. A., Peng, C. Y., Nanayakkara, A., Challacombe, M., Gill, P. M. W., Johnson, B., Chen, W., Wong, M. W., Gonzalez, C., and Pople, J. A.: Gaussian 09, Revision D.01; Gaussian, Inc.: Wallingford, CT, 2009.

Fukui, K.: The path of chemical reactions - the IRC approach, Acc. Chem. Res., 14, 363-368, https://doi.org/10.1021/ar00072a001, 1981.

Georgievskii, Y., and Klippenstein, S. J.: Long-range transition state theory, J. Chem. Phys., 122, 194103-194119, https://doi.org/10.1063/1.1899603, 2005.

Giorio, C., Campbell, S. J., Bruschi, M., Tampieri, F., Barbon, A., Toffoletti, A., Tapparo, A., Paijens, C., Wedlake, A. J., Grice, P., Howe, D. J., and Kalbere, M.: Online quantification of Criegee intermediates of α-pinene ozonolysis by stabilization with spin traps and proton-transfer reaction mass spectrometry detection, J. Am. Chem. Soc., 139, 3999-4008, https://doi.org/10.1021/jacs.6b10981, 2017.

Gong, Y., and Chen, Z.: Quantification of the role of stabilized Criegee intermediates in the

https://doi.org/10.5194/acp-2022-376
Preprint. Discussion started: 8 June 2022

formation of aerosols in limonene ozonolysis, Atmos. Chem. Phys., 21, 813-829, https://doi.org/10.5194/acp-21-813-2021, 2021.

Huang, H. L., Chao, W., and Lin, J. J. M.: Kinetics of a Criegee intermediate that would survive high humidity and may oxidize atmospheric SO_2, Proc. Natl. Acad. Sci. U.S.A., 112, 10857-10862, https://doi.org/ 10.1073/pnas.1513149112, 2015.

Johnson, D., and Marston, G.: The gas-phase ozonolysis of unsaturated volatile organic compounds in the troposphere, Chem. Soc. Rev., 37, 699-716, https://doi.org/10.1039/B704260B, 2008.

Johnson, D., Lewin, A. G., and Marston, G.: The effect of Criegee-intermediate scavengers on the OH yield from the reaction of ozone with 2-methylbut-2-ene, J. Phys. Chem. A, 105, 2933-2935, https://doi.org/10.1021/jp003975e, 2001.

Khan, M. A. H., Percival, C. J., Caravan, R. L., Taatjes, C. A., and Shallcross, D. E.: Criegee intermediates and their impacts on the troposphere, Environ. Sci.: Processes Impacts, 20, 437-453, https://doi.org/10.1039/C7EM00585G, 2018.

Lester, M. I., and Klippenstein, S. J.: Unimolecular decay of Criegee intermediates to OH radical products: prompt and thermal decay processes, Acc. Chem. Res., 51, 978-985, https://doi.org/10.1021/acs.accounts.8b00077, 2018.

Lin, J. J. M., and Chao, W.: Structure-dependent reactivity of Criegee intermediates studied with spectroscopic methods, Chem. Soc. Rev., 46, 7483-7497, https://doi.org/10.1039/c7cs00336f, 2017.

Lin, X., Meng, Q., Feng, B., Zhai, Y., Li, Y., Yu, Y., Li, Z., Shan, X., Liu, F., Zhang, L., and Sheng, L.: Theoretical study on Criegee intermediate's role in ozonolysis of acrylic acid, J. Phys. Chem. A, 123, 1929-1936, https://doi.org/10.1021/acs.jpca.8b11671, 2019.

Liu, F., Beames, J. M., Petit, A. S., McCoy, A. B., and Lester, M. I.: Infrared-driven unimolecular reaction of CH_3CHOO Criegee intermediates to OH radical products, Science, 345, 1596-1598, https://doi.org/10.1126/science.1257158, 2014.

Liu, L., Bei, N., Wu, J., Liu, S., Zhou, J., Li, X., Yang, Q., Feng, T., Cao, J., Tie, X., and Li, G.: Effects of stabilized Criegee intermediates (sCIs) on sulfate formation: a sensitivity analysis during summertime in Beijing-Tianjin-Hebei (BTH), China, Atmos. Chem. Phys., 19, 13341-13354, https://doi.org/10.5194/acp-19-13341-2019, 2019.

Long, B., Bao, J. L., and Truhlar, D. G.: Atmospheric chemistry of Criegee intermediates: unimolecular reactions and reactions with water, J. Am. Chem. Soc., 138, 14409-14422, https://doi.org/10.1021/jacs.6b08655, 2016.

Long, B., Bao, J. L., and Truhlar, D. G.: Unimolecular reaction of acetone oxide and its reaction with water in the atmosphere, Proc. Natl. Acad. Sci. U.S.A., 115, 6135-6140, https://doi.org/10.1073/pnas.1804453115, 2018.

Long, B., Cheng, J. R., Tan, X. F., and Zhang, W. J.: Theoretical study on the detailed reaction mechanisms of carbonyl oxide with formic acid, J. Mol. Struc.: Theochem, 916, 159-167, https://doi.org/10.1016/j.theochem.2009.09.028, 2009.

Mendes, J., Zhou, C. W., and Curran, H. J.: Theoretical chemical kinetic study of the H-atom abstraction reactions from aldehydes and acids by H atoms and OH, HO_2, and CH_3 radicals, J. Phys. Chem. A, 118, 12089-12104, https://doi.org/10.1021/jp5072814, 2014.

Neeb, P., Horie, O., and Moortgat, G. K.: The ethene-ozone reaction in the gas phase, J. Phys. Chem. A, 102, 6778-6785, https://doi.org/10.1021/jp981264z, 1998.

https://doi.org/10.5194/acp-2022-376
Preprint. Discussion started: 8 June 2022

Atmospheric Chemistry and Physics Discussions

729 Novelli, A., Vereecken, L., Lelieveld, J., and Harder, H.: Direct observation of OH formation from
730 stabilised Criegee intermediates, Phys. Chem. Chem. Phys., 16, 19941-19951,
731 https://doi.org/10.1039/c4cp02719a, 2014.
732 Osborn, D. L., and Taatjes, C. A.: The physical chemistry of Criegee intermediates in the gas
733 phase, Int. Rev. Phys. Chem., 34, 309-360, https://doi.org/10.1080/0144235X.2015.1055676,
734 2015.
735 Paulot, F., Wunch, D., Crounse, J. D., Toon, G. C., Millet, D. B., DeCarlo, P. F., Vigouroux, C.,
736 Deutscher, N. M., Abad, G. G., Notholt, J., Warneke, T., Hannigan, J. W., Warneke, C., de
737 Gouw, J. A., Dunlea, E. J., Mazière, M. D., Griffith, D. W. T., Bernath, P., Jimenez, J. L., and
738 Wennberg, P. O.: Importance of secondary sources in the atmospheric budgets of formic and
739 acetic acids, Atmos. Chem. Phys., 11, 1989-2013, https://doi.org/10.5194/acp-11-1989-2011,
740 2011.
741 Peltola, J., Seal, P., Inkilä, A., and Eskola, A.: Time-resolved, broadband UV-absorption
742 spectrometry measurements of Criegee intermediate kinetics using a new photolytic
743 precursor: unimolecular decomposition of CH_2OO and its reaction with formic acid, Phys.
744 Chem. Chem. Phys., 22, 11797-11808, https://doi.org/10.1039/d0cp00302f, 2020.
745 Porterfield, J. P., Lee, K. L. K., Dell'Isola, V., Carroll, P. B., and McCarthy, M. C.:
746 Characterization of the simplest hydroperoxide ester, hydroperoxymethyl formate, a
747 precursor of atmospheric aerosols, Phys. Chem. Chem. Phys., 21, 18065-18070,
748 https://doi.org/10.1039/c9cp03466h, 2019.
749 Riva, M., Budisulistiorini, S. H., Zhang, Z., Gold, A., Thornton, J. A., Turpin, B. J., and Surratt, J.
750 D.: Multiphase reactivity of gaseous hydroperoxide oligomers produced from isoprene
751 ozonolysis in the presence of acidified aerosols, Atmos. Environ., 152, 314-322,
752 https://doi.org/10.1016/j.atmosenv.2016.12.040, 2017.
753 Rousso, A. C., Hansen, N., Jasper, A. W., and Ju, Y.: Low-temperature oxidation of ethylene by
754 ozone in a jet-stirred reactor, J. Phys. Chem. A, 122, 8674-8685,
755 https://doi.org/10.1021/acs.jpca.8b06556, 2018.
756 Sadezky, A., Winterhalter, R., Kanawati, B., Rompp, A., Spengler, B., Mellouki, A., Bras, G. L.,
757 Chaimbault, P., and Moortgat, G. K.: Oligomer formation during gas-phase ozonolysis of
758 small alkenes and enol ethers: new evidence for the central role of the Criegee Intermediate
759 as oligomer chain unit, Atmos. Chem. Phys., 8, 2667-2699,
760 https://doi.org/10.5194/acp-8-2667-2008, 2008.
761 Sakamoto, Y., Inomata, S., and Hirokawa, J.: Oligomerization reaction of the Criegee intermediate
762 leads to secondary organic aerosol formation in ethylene ozonolysis, J. Phys. Chem. A, 117,
763 12912-12921, https://doi.org/10.1021/jp408672m, 2013.
764 Sakamoto, Y., Yajima, R., Inomatad, S., and Hirokawa, J.: Water vapour effects on secondary
765 organic aerosol formation in isoprene ozonolysis, Phys. Chem. Chem. Phys., 19, 3165-3175,
766 https://doi.org/10.1039/c6cp04521a, 2017.
767 Sipilä, M., Jokinen, T., Berndt, T., Richters, S., Makkonen, R., Donahue, N. M., Mauldin Iii, R. L.,
768 Kurtén, T., Paasonen, P., Sarnela, N., Ehn, M., Junninen, H., Rissanen, M. P., Thornton, J.,
769 Stratmann, F., Herrmann, H., Worsnop, D. R., Kulmala, M., Kerminen, V. M., and Petäjä, T.:
770 Reactivity of stabilized Criegee intermediates (sCIs) from isoprene and monoterpene
771 ozonolysis toward SO_2 and organic acids, Atmos. Chem. Phys., 14, 12143-12153,
772 https://doi.org/10.5194/acp-14-12143-2014, 2014.

https://doi.org/10.5194/acp-2022-376
Preprint. Discussion started: 8 June 2022

Atmospheric Chemistry and Physics Discussions

So, S., Wille, U., and Silva, G. D.: Atmospheric chemistry of enols: a theoretical study of the vinyl alcohol + OH + O_2 reaction mechanism, Environ. Sci. Technol., 48, 6694-6701, https://doi.org/10.1021/es500319q, 2014.

Stavrakou, T., Müller, J. F., Peeters, J., Razavi, A., Clarisse, L., Clerbaux, C., Coheur, P. F., Hurtmans, D., Mazière, M. D., Vigouroux, C., Deutscher, N. M., Griffith, D. W. T., Jones, N., and Paton-Walsh, C.: Satellite evidence for a large source of formic acid from boreal and tropical forests, Nat. Geosci., 5, 26-30, https://doi.org/10.1038/ngeo1354, 2012.

Taatjes, C. A., Khan, M. A. H., Eskola, A. J., Percival, C. J., Osborn, D. L., Wallington, T. J., and Shallcross, D. E.: Reaction of perfluorooctanoic acid with Criegee intermediates and implications for the atmospheric fate of perfluorocarboxylic acids, Environ. Sci. Technol., 53, 1245-1251, https://doi.org/10.1021/acs.est.8b05073, 2019.

Taatjes, C. A., Welz, O., Eskola, A. J., Savee, J. D., Scheer, A. M., Shallcross, D. E., Rotavera, B., Lee, E. P. F., Dyke, J. M., Mok, D. K. W., Osborn, D. L., and Percival, C. J.: Direct measurements of conformer-dependent reactivity of the Criegee intermediate CH_3CHOO, Science, 340, 177-180, https://doi.org/10.1126/science.1234689, 2013.

Taatjes, C. A.: Criegee intermediates: what direct production and detection can teach us about reactions of carbonyl oxides, Annu. Rev. Phys. Chem., 68, 183-207, https://doi.org/10.1146/annurev-physchem-052516-050739, 2017.

Tobias, H. J., and Ziemann, P. J.: Kinetics of the gas-phase reactions of alcohols, aldehydes, carboxylic acids, and water with the C13 stabilized Criegee intermediate formed from ozonolysis of 1-tetradecene, J. Phys. Chem. A, 105, 6129-6135, https://doi.org/10.1021/jp004631r, 2001.

Truhlar, D. G., Hase, W. L., and Hynes, J. T.: Current status of transition-state theory, J. Phys. Chem., 87, 2664-2682, https://doi.org/10.1021/jp953748q, 1996.

Vansco, M. F., Zuraski, K., Winiberg, F. A. F., Au, K., Trongsiriwat, N., Walsh, P. J., Osborn, D. L., Percival, C. J., Klippenstein, S. J., Taatjes, C. A., Lester, M. I., and Caravan, R. L.: Functionalized hydroperoxide formation from the reaction of methacrolein-oxide, an isoprene-derived Criegee intermediate, with formic acid: experiment and theory, Molecules, 26, 3058-3072, https://doi.org/10.3390/molecules26103058, 2021.

Vereecken, L., Harder, H., and Novelli, A.: The reaction of Criegee intermediates with NO, RO_2, and SO_2, and their fate in the atmosphere, Phys. Chem. Chem. Phys., 14, 14682-14695, https://doi.org/10.1039/c2cp42300f, 2012.

Vereecken, L.: The reaction of Criegee intermediates with acids and enols, Phys. Chem. Chem. Phys., 19, 28630-28640, https://doi.org/10.1039/c7cp05132h, 2017.

Wang, S., Newland, M. J., Deng, W., Rickard, A. R., Hamilton, J. F., Muñoz, A., Ródenas, M., Vázquez, M. M., Wang, L., and Wang, X.: Aromatic photo-oxidation, a new source of atmospheric acidity, Environ. Sci. Technol., 54, 7798-7806, https://doi.org/10.1021/acs.est.0c00526, 2020.

Welz, O., Eskola, A. J., Sheps, L., Rotavera, B., Savee, J. D., Scheer, A. M., Osborn, D. L., Lowe, D., Booth, A. M., Xiao, P., Khan, M. A. H., Percival, C. J., Shallcross, D. E., and Taatjes, C. A.: Rate coefficients of C(1) and C(2) Criegee intermediate reactions with formic and acetic Acid near the collision limit: direct kinetics measurements and atmospheric implications, Angew. Chem. Int. Ed., 53, 4547-4550, https://doi.org/10.1002/anie.201400964, 2014.

Yin, C., and Takahashi, K.: How does substitution affect the unimolecular reaction rates of

https://doi.org/10.5194/acp-2022-376
Preprint. Discussion started: 8 June 2022

Atmospheric Chemistry and Physics Discussions

817 Criegee intermediates? Phys. Chem. Chem. Phys., 19, 12075-12084,
818 https://doi.org/10.1039/c7cp01091e, 2017.
819 Yu, S.: Role of organic acids (formic, acetic, pyruvic and oxalic) in the formation of cloud
820 condensation nuclei (CCN): a review, Atmos. Res., 53, 185-217,
821 https://doi.org/10.1016/S0169-8095(00)00037-5, 2000.
822 Zhang, P., Wang, W., Zhang, T., Chen, L., Du, Y., Li, C., and Lv, J.: Theoretical study on the
823 mechanism and kinetics for the self-reaction of $C_2H_5O_2$ radicals, J. Phys. Chem. A, 116,
824 4610-4620, https://doi.org/10.1021/jp301308u, 2012.
825 Zhao, R., Kenseth, C. M., Huang, Y., Dalleska, N. F., Kuang, X. M., Chen, J., Paulson, S. E., and
826 Seinfeld, J. H.: Rapid aqueous-phase hydrolysis of ester hydroperoxides arising from Criegee
827 intermediates and organic acids, J. Phys. Chem. A, 122, 5190-5201,
828 https://doi.org/10.1021/acs.jpca.8b02195, 2018.
829 Zhao, Y., and Truhlar, D. G.: The M06 suite of density functionals for main group
830 thermochemistry, thermochemical kinetics, noncovalent interactions, excited states, and
831 transition elements: two new functionals and systematic testing of four M06-class functionals
832 and 12 other functionals, Theor. Chem. Acc., 120, 215-241,
833 https://doi.org/10.1007/s00214-007-0310-x, 2008.
834 Zhao, Y., Wingen, L. M., Perraud, V., Greaves, J., and Finlayson-Pitts, B. J.: Role of the reaction
835 of stabilized Criegee intermediates with peroxy radicals in particle formation and growth in
836 air, Phys. Chem. Chem. Phys., 17, 12500-12514, https://doi.org/10.1039/c5cp01171j, 2015.
837 Zhou, S., Joudan, S., Forbes, M. W., Zhou, Z., and Abbatt, J. P. D.: Reaction of condensed-phase
838 Criegee intermediates with carboxylic acids and perfluoroalkyl carboxylic acids, Environ. Sci.
839 Technol. Lett., 6, 243-250, https://doi.org/10.1021/acs.estlett.9b00165, 2019.
840